Nano Research 2018, 11(2): 707–721
https://doi.org/10.1007/s12274-017-1680-6
Research Article
ISSN 1998-0124
CN 11-5974/O4

Three-layer phosphorene-metal interfaces

Xiuying Zhang[1,§], Yuanyuan Pan[1,§], Meng Ye[1], Ruge Quhe[2], Yangyang Wang[1,3], Ying Guo[4], Han Zhang[1], Yang Dan[1], Zhigang Song[1], Jingzhen Li[1], Jinbo Yang[1,5], Wanlin Guo[6], and Jing Lu[1,5] (✉)

[1] *State Key Laboratory for Mesoscopic Physics and Department of Physics, Peking University, Beijing 100871, China*
[2] *State Key Laboratory of Information Photonics and Optical Communications and School of Science, Beijing University of Posts and Telecommunications, Beijing 100876, China*
[3] *Nanophotonics and Optoelectronics Research Center, Qian Xuesen Laboratory of Space Technology, China Academy of Space Technology, Beijing 100094, China*
[4] *School of Physics and Telecommunication Engineering, Shaanxi Sci-Tech University, Hanzhong 723001, China*
[5] *Collaborative Innovation Center of Quantum Matter, Beijing 100871, China*
[6] *Key Laboratory for Intelligent Nano Materials and Devices of the Ministry of Education, Nanjing University of Aeronautics and Astronautics, Nanjing 210016, China*
[§] *Xiuying Zhang and Yuanyuan Pan contributed equally to this work.*

Received: 8 January 2017
Revised: 10 May 2017
Accepted: 16 May 2017

KEYWORDS

three-layer phosphorene, interfacial properties, Schottky barrier height, density functional theory, quantum transport simulation

ABSTRACT

Phosphorene has attracted much attention recently as an alternative channel material in nanoscale electronic and optoelectronic devices due to its high carrier mobility and tunable direct bandgap. Compared with monolayer (ML) phosphorene, few-layer (FL) phosphorene is easier to prepare, is more stable in experiments, and is expected to form a smaller Schottky barrier height (SBH) at the phosphorene-metal interface. Using *ab initio* electronic structure calculations and quantum transport simulations, we perform a systematic study of the interfacial properties of three-layer (3L) phosphorene field effect transistors (FETs) contacted with several common metals (Al, Ag, Au, Cu, Ti, Cr, Ni, and Pd) for the first time. The SBHs obtained in the vertical direction from projecting the band structures of the 3L phosphorene-metal systems to the left bilayer (2L) phosphorenes are comparable with those obtained in the lateral direction from the quantum transport simulations for 2L phosphorene FETs. The quantum transport simulations for the 3L phosphorene FETs show that 3L phosphorene forms n-type Schottky contacts with electron SBHs of 0.16 and 0.28 eV in the lateral direction, when Ag and Cu are used as electrodes, respectively, and p-type Schottky contacts with hole SBHs of 0.05, 0.11, 0.20, 0.30, 0.30, and 0.31 eV in the lateral direction when Cr, Pd, Ni, Ti, Al, and Au are used as electrodes, respectively. The calculated polarity and SBHs of the 3L phosphorene FETs are generally in agreement with the available experiments.

Address correspondence to jinglu@pku.edu.cn

1 Introduction

Phosphorene, a new two-dimensional (2D) elemental material, was isolated from black phosphorus crystals in 2014 [1–5]. Phosphorene shows a finite direct band gap that varies from 0.3 (bulk) to 2.0 eV (monolayer) as a function of layer number and exhibits in-plane anisotropic properties [4, 6, 7]. Field effect transistors (FETs) with phosphorene as the channel material have high carrier mobilities of up to 1,000 $cm^2 \cdot V^{-1} \cdot s^{-1}$ and high on-off current ratios of up to 10^5 [1–3, 8–10]. All these properties make it a promising candidate for future high-performance nanoelectronic and nanooptoelectronics applications. It is difficult for 2D materials to be doped through substitutional doping methods [11, 12], and the phosphorene FETs typically fabricated in experiments have phosphorene-metal electrode direct contacts, in which Schottky barriers are usually formed at the metal-phosphorene junction [10]. Schottky barriers always decrease charge transport in devices [4, 13], and thus a small Schottky barrier height (SBH) or even an Ohmic contact at the metal-semiconductor interface is crucial for designing high-performance phosphorene devices.

Few-layer (FL) phosphorene has three advantages over monolayer (ML) phosphorene. First, phosphorene thicker than 2 nm (about 3 layers) is less sensitive to the environment than phosphorene thinner than 2 nm [3]. Second, FL phosphorene is more easily prepared than ML, and thus is more frequently used as the channel materials in experiments [6, 12]. Third, FL phosphorene-metal systems are expected to have smaller SBHs than their ML phosphorene counterparts because FL phosphorenes have smaller band gaps [14–16]. FL phosphorene FETs have been fabricated with Al, Au, Ti, Cr, Ni, and Pd contacts and the layer number dependence of the phosphorene-Ni SBH has been studied experimentally [2, 6, 9, 17–25]. The interfacial properties between ML phosphorene and metal [14, 26, 27] have also been studied theoretically. However, there has been no systematic study of the interfacial properties of FL phosphorene-metal systems with a given layer number.

In this paper, the interfacial properties of three-layer (3L) phosphorene-metal (Ag, Al, Au, Pd, Cu, Ti, Cr, and Ni) interfaces in an FET configuration are investigated systematically for the first time using *ab initio* electronic structure calculations and quantum transport simulations. There is no Schottky barrier between the contacted phosphorene layer (the contact layer) and the metal surface in the vertical direction due to strong band hybridization. However, there exists a Schottky barrier between the contacted layer and the unexposed bilayer (2L) phosphorene because of the identifiable band structure of the latter. When projected to unexposed 2L phosphorenes, the SBHs obtained in the vertical direction from 3L phosphorene-metal system band structures are comparable with those obtained in the lateral direction from quantum transport simulations on 2L phosphorene FETs [28]. Quantum transport simulations reveal that 3L phosphorene FETs with Ag and Cu electrodes are n-type with electron SBHs of 0.16 and 0.28 eV in the lateral direction, respectively. Those with Cr, Pd, Ni, Ti, Al, and Au electrodes are p-type with hole SBHs of 0.05, 0.11, 0.20, 0.30, 0.30, and 0.31 eV in the lateral direction, respectively. Consistently, the experimental results also indicate that FL phosphorene is n-doped with Cu adatoms [29] and p-doped with Au, Ti, Ni, and Pd electrodes [2–4, 6, 17]. Furthermore, the experimental electron/hole (0.40/0.21 eV) SBH of the 3L phosphorene FET with Ni electrode [2] is also in agreement with our calculated value (0.48 eV for electron and 0.20 eV for hole).

2 Methods

The supercells chosen to model the 3L phosphorene-metal surface systems are constructed from a slab of five layers of metal atoms with 3L phosphorene absorbed on one side of the metal surfaces, as used in previous work [30–32]. A vacuum buffer space of at least 12 Å is set to avoid spurious interactions, as shown in Fig. 1(a). The initial lattice constant of 3L phosphorene are set as $\boldsymbol{a}$ = 3.33 Å and $\boldsymbol{b}$ = 4.51 Å as reported by Qiao et al. [33]. We adapted $\sqrt{\boldsymbol{a}^2+\boldsymbol{b}^2} \times \sqrt{(2\boldsymbol{a})^2+\boldsymbol{b}^2}$ 3L phosphorene supercells to 2 × 2 Al (110), Ag (110), Au (110), and Cr (110) surface supercells, $3\boldsymbol{a} \times \boldsymbol{b}$ 3L phosphorene supercells to $4 \times \sqrt{3}$ Ni(111) and Cu (111) surface supercells, and $2\boldsymbol{a} \times 3\boldsymbol{b}$ and $5\boldsymbol{a} \times \boldsymbol{b}$ 3L phosphorene supercells to $2\sqrt{3} \times 3$ Ti (0001) and $6 \times \sqrt{3}$ Pd (111) surface supercells, respectively. The corresponding lattice constant mismatches are all

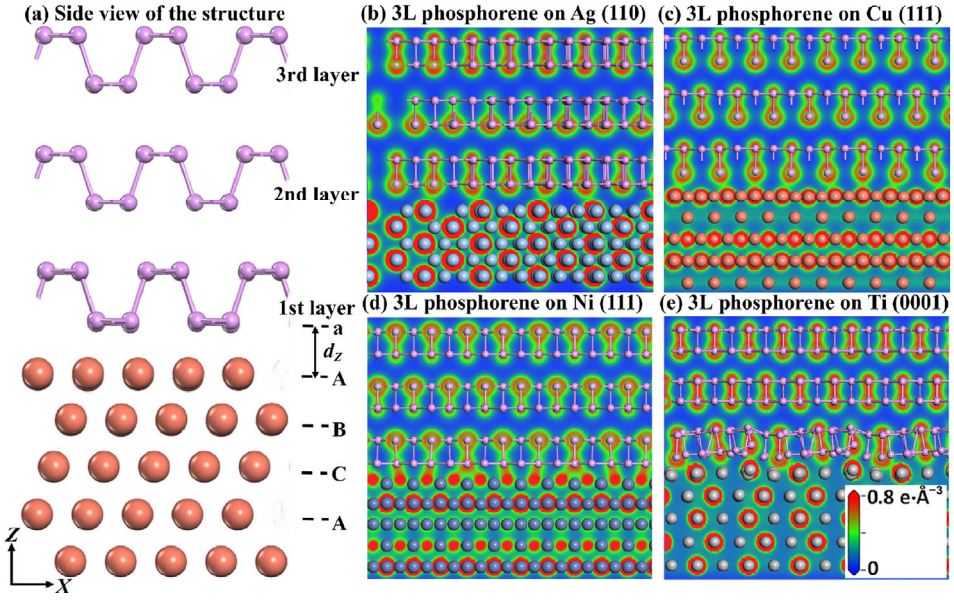

Figure 1 (a) Schematic structure of 3L phosphorene (purple ball) on the metal surface (orange ball). Contour plots of total electron distribution of 3L phosphorene in contact with the (b) Ag, (c) Cu, (d) Ni and (e) Ti surfaces. The purple balls represent P atoms, and the other kinds of color balls represent metal atoms, respectively.

less than 2%, as shown in Table 1. We only allow the position of phosphorous atoms and the top two layers (layer A and B in Fig. 1(a)) of metal atoms to relax and keep the bottom three metal layers unchanged when optimizing the geometry.

During geometry optimization and electronic structure calculations, we use a plane-wave basis set with a cut-off energy of 400 eV and projector augmented wave (PAW) pseudopotential [34], and a fine *k*-mesh density of 0.02 Å^{-1} under the Monkhorst-Pack method [35] is sampled in the Brillouin zone, as implemented in the Vienna *ab initio* simulation package (VASP) code [36, 37]. The atoms are relaxed until the residual force on each atom is less than 0.01 eV·Å^{-1}, and the

Table 1 Calculated interlayer properties of 3L phosphorene-metal contacts

	$\bar{\varepsilon}$ [a] (%)	d_Z [b] (Å)	d_{min} [c] (Å)	$(r_P + r_M)$ [d] (Å)	E_b [e] (eV)	W [f] (eV)	W_M [f] (eV)	$\Phi_{23,V}^{e,3L}$ [g] (eV)	$\Phi_{23,V}^{h,3L}$ [g] (eV)	$\Phi_{T,L}^{e,3L}$ [h] (eV)	$\Phi_{T,L}^{h,3L}$ [h] (eV)	E_g [i] (eV)
Al	0.52	2.49	2.59	2.37	0.44	4.38	3.96	0.37	0.41	0.47	0.30	0.77
Ag	1.12	2.43	2.59	2.39	0.46	4.59	4.16	0.39	0.32	0.16	0.45	0.61
Cu	1.39	2.30	2.36	2.23	0.68	4.92	4.78	0.00	0.00	0.28	0.43	0.71
Au	1.00	2.38	2.48	2.35	0.86	4.97	5.04	0.40	0.30	0.33	0.31	0.64
Pd	0.96	2.11	2.28	2.55	1.18	5.10	5.26	0.36	0.14	0.55	0.11	0.66
Ni	1.67	1.73	2.18	2.21	1.41	5.00	5.07	0.44	0.13	0.48	0.20	0.68
Ti	1.39	1.85	2.42	2.47	1.48	4.63	4.45	0.38	0.24	0.33	0.30	0.63
Cr	1.02	1.69	2.23	2.33	2.03	4.83	4.64	0.25	0.44	0.63	0.05	0.68

[a] $\bar{\varepsilon}$ is the average lattice constant mismatch between the metal surfaces and 3L phosphorene. [b] The equilibrium distance d_Z is the average distance between the contact 3L phosphorene-metal interfaces in the vertical direction. [c] d_{min} is the minimum atom-to-atom distance from the phosphorous atoms to the metal atoms. [d] $(r_P + r_M)$ is the sum of the single-bond covalent radii for phosphorous and metal atoms. [e] The binding energy E_b is the energy per phosphorus atom to remove 3L phosphorene from the metal surface. [f] W_M and W are the calculated WF for clean metal surface and the 3L phosphorene-metal system, respectively. [g] ($\Phi_{23,V}^{e/h,3L}$) is the SBH of the electron (hole) in the vertical direction when the charge carriers travel from the contacted phosphorene layer to the unexposed 2L phosphorene. [h] ($\Phi_{T,L}^{e/h,3L}$) is the transport SBH of the electron (hole) of the 3L phosphorene FET in the lateral direction. [i] E_g is the transmission gap of the 3L phosphorene FET.

total energies converge to within 1×10^{-5} eV/atom. Two corrections are taken into account during the relaxation and electronic calculation periods. The first one is the van der Waals (vdW) interaction with the vdW-DF level of the optB88 exchange-correlation functional (optB88-vdW) [38]. The second is the dipole correction, which is used to remove the spurious interaction caused by the dipole moments of periodic images in the *Z* direction as the result of the asymmetry of interfaces. The total electron density is calculated in CASTEP code using a plane-wave basis set with a cut-off energy of 280 eV and an ultrasoft pseudopotential [39].

A two-probe model of 3L phosphorene FET (Fig. 7) is built, and 3L phosphorene is used as the channel material with a channel length of 5 nm in the transport direction. The electrodes adopt the optimized 3L phosphorene-metal interfacial structure. The lengths of the left and right electrodes are semi-infinite. The transmission spectra and local device density of states (LDDOS) are calculated by using density functional theory coupled with a nonequilibrium Green's function (NEGF) method, which is implemented in the Atomistix ToolKit (ATK) 2016 package [30, 41]. The transmission coefficient $T^{k_{//}}(E)$ ($k_{//}$), which is a reciprocal lattice vector point along a surface-parallel direction (orthogonal to the transmission direction) in the irreducible Brillouin zone (IBZ)), is calculated as

$$T^{k_{//}}(E)=\mathrm{Tr}\left[\Gamma_{\mathrm{L}}^{k_{//}}(E)G^{k_{//}}(E)\Gamma_{\mathrm{R}}^{k_{//}}(E)G^{k_{//}\dagger}(E)\right] \quad (1)$$

where $G^{k_{//}}$ is the retarded (advanced) Green's function, and $\Gamma_{\mathrm{L/R}}^{k_{//}}(E)=i(\sum_{\mathrm{L/R}}^{r,k_{//}}-\sum_{\mathrm{L/R}}^{a,k_{//}})$ represents the level broadening due to left electrodes and right electrodes expressed in terms of the electrode self-energies $\sum_{\mathrm{L/R}}^{k_{//}}$, which reflects the influence of the electrodes on the scattering region [42]. The transmission function at a given energy $T(E)$ is averaged over different $k_{//}$ in the IBZ. A single-ζ plus polarization (SZP) basis set is employed. The real-space mesh cutoff is 75 Hartrees, and the temperature is set at 300 K. The electronic structure of the electrodes and central region are calculated with a Monkhorst–Pack [34] 50 × 1 × 50 and 50 × 1 × 1 *k*-point grid, respectively. Generalized gradient approximation (GGA) of the Perdew-Burke-Ernzerhof (PBE) form [43] of the exchange-correlation functional is applied in the transport simulation.

The optB88-vdW and PBE functionals we used to calculate the band gap are appropriate because, in the FET configuration, both the semiconductors under the metal electrode and channel semiconductors are heavily doped by the metal electrode and gate voltage, respectively. In this case, the many-electron effect is strongly depressed, and the single-electron approximation becomes a good approximation [15, 44]. As a result, the band gap given by the optB88-vdW and PBE methods is comparable with the experimental value. For example, the calculated transmission gaps for the ML/2L/3L phosphorene FETs (about 1/0.7/0.65 eV) [14, 28] with the variable of metal electrodes are comparable with the experimental transmission gaps of 0.99/0.70/0.65 eV with Ni electrodes [2].

3 Results and discussion

3.1 Interfacial structures

The initial position of the first layer phosphorene (the contacted layer) relative to the metal surfaces for 3L phosphorene is taken from the stable ML phosphorene-metal structures [14]. The optimized 3L phosphorene-metal structures (Fig. 2) show small changes in the structures of 3L phosphorene on Al, Ag, Au, Cu, and Pd, but the contacted phosphorene layer is distorted on Ti, Ni, and Cr. The calculated key parameters of 3L phosphorene-metal systems are listed in Table 1. We define the binding energy E_{b} of the 3L phosphorene-metal systems as

$$E_{\mathrm{b}}=\left(E_{\mathrm{P}}+E_{\mathrm{M}}-E_{\mathrm{P\text{-}M}}\right)/N \quad (2)$$

where E_{P}, E_{M} and $E_{\mathrm{P\text{-}M}}$ are the relaxed energy for pure 3L phosphorenes, the pure metal surfaces, and 3L phosphorene-metal systems, respectively, and N is the number of phosphorus atoms in direct contacted with the metals (layer a in Fig. 1(a)). The interlayer distance d_Z is the average distance between the innermost phosphorene layer (layer a) and the outmost metal layer (layer A) in the *Z*-direction (normal to the surface) as shown in Fig. 1 (a), and d_{min} is the minimum atom-to-atom distance between the phosphorus atoms and the metal atoms.

The binding energy of 3L phosphorene on the Ag, Al, Au, and Cu surfaces is smaller, with values of ~ 0.44–0.86 eV, accompanied by larger interlayer (2.30 <

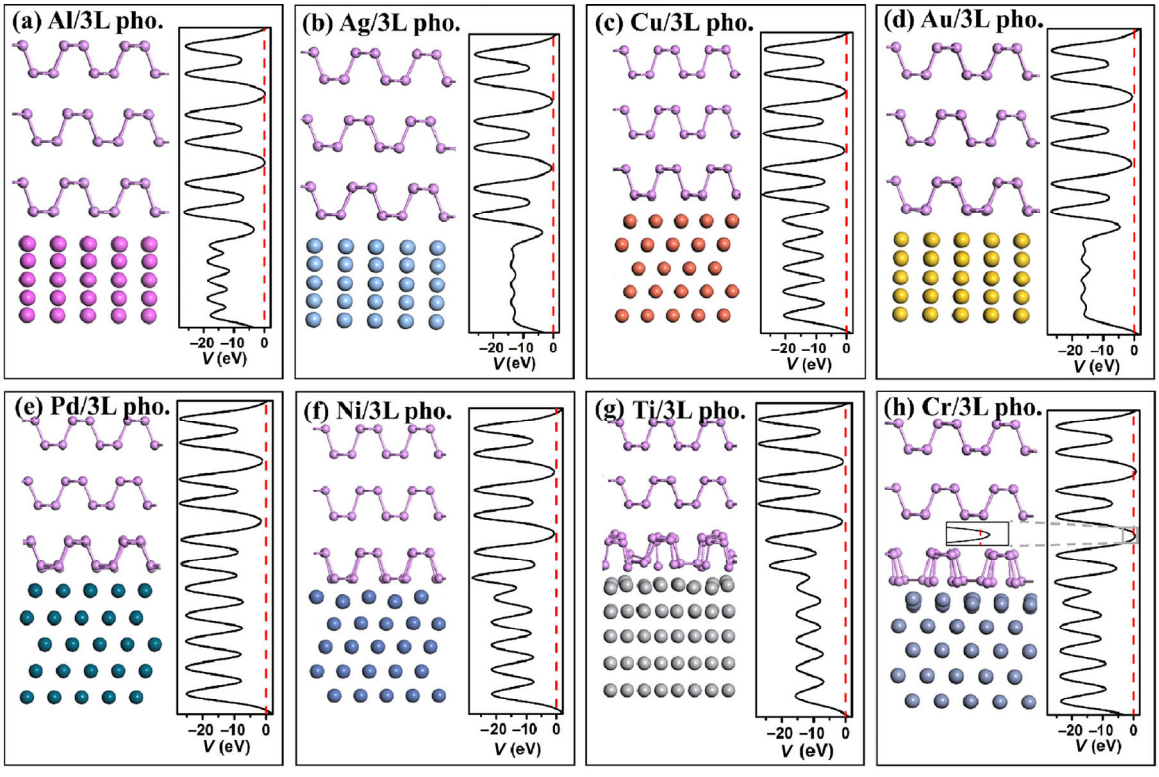

Figure 2 Side view of the most stable structure and total electrostatic potential distribution in planes normal to the interface of 3L phosphorene (pho.) on (a) Al, (b) Ag, (c) Cu, (d) Au, (e) Pd, (f) Ni, (g) Ti and (h) Cr surfaces. The Fermi level is set to zero. Inset in (h) is the zoom of the region in the grey box.

d_Z < 2.49 Å) and minimum atom-to-atom distances (2.36 < d_{min} < 2.59 Å). In contrast, the binding energy of 3L phosphorene on the Pd, Ni, Cr, and Ti surfaces is larger, with values of ~ 1.18–2.03 eV, accompanied by smaller interlayer (1.69 < d_Z < 2.11 Å) and minimum atom-to-atom distances (2.18 < d_{min} < 2.42 Å).

These differences are attributed to the fact that Ti and Ni have two unpaired electrons, but Al, Ag, Au, and Cu have only one. Thus, Ti and Ni can form more bonds with phosphorus than Al, Ag, Au, and Cu. Cr has six unpaired electrons, so the 3L phosphorene-Cr system has the largest binding energy and the smallest interlayer distance (d_Z). The outermost orbital of Pd is fully occupied ($4d^{10}$), but the phosphorene-Pd system has a respectively larger binding energy (1.18 eV) than phosphorene-Al, -Ag, -Au, and -Cu. This difference can be attributed to the fact that the 4d orbital of Pd is hybridized with the outer 5s orbital when contacted with phosphorene, resulting in two unpaired electrons [45]. However, hybridization consumes energy, so the binding energy of 3L phosphorene with Pd is smaller than with Ni and Ti.

We can classify the 3L phosphorene-metal systems into two categories according to their structural distortion degree and binding strength: Weak chemical bonding systems (phosphorene with Al, Ag, Au, and Cu) and strong chemical bonding systems (phosphorene with Pd, Cr, Ni, and Ti). A Bader charge analysis determined the bond character, and small charge transfers of 0.13e, 0.11e, and 0.07e are found for phosphorene-Ti, Cr, and Al systems, respectively, indicating the existence of a weak ionic bond between phosphorene and Ti, Cr, and Al. The dominant interaction between phosphorene and metal should thus be a covalent bond, as will be mentioned in the band structure section. The binding energy values of 3L phosphorene with metals are all larger than those of ML phosphorene with metals [14]. This difference can be attributed to the smaller band gap of 3L phosphorene; thus, carriers need less energy to transfer between the metals and 3L phosphorene than between the metals and ML phosphorene.

3.2 Electronic structure

The band structures of the 3L phosphorene-metal systems projected to the 3L phosphorenes (Fig. 3) are strongly hybridized [30, 46–48], proving that 3L phosphorene combines covalently with metals. The band structures of 3L phosphorene-metal systems projected to the contacted phosphorene layer are destroyed (Fig. 4), confirming the formation of covalent bonds between the contacted phosphorene layer and the metals. Besides, some of the contacted phosphorene layer states cross the Fermi level (E_f), indicating metallization of the contacted phosphorene layers [45, 49–52]. The hybridization degree of the band structures projected to the contacted phosphorene layer is more intense when 3L phosphorene contacted Pd, Ni, Cr, and Ti than for Al, Ag, Au, and Cu. This hybridization degree of the band structures is in accordance with the structural distortion degree and the binding strength.

The band structures projected to the left 2L (the unexposed 2L) phosphorene are not destroyed so intensely as the contacted layer (Fig. 5), and the band structure of pure 2L phosphorene is also provided for comparison in Fig. 5. The unexposed 2L phosphorene remains a semiconductor when 3L phosphorene contacts with Al, Ag, Au, Cr, Ti, Ni, and Pd, with band gaps of 0.78, 0.71, 0.70, 0.69, 0.62, 0.57, and 0.50 eV, respectively, which are comparable to the band gap of pure 2L phosphorene (0.75 eV). However, the band structure of the 3L phosphorene-Cu system projected to the unexposed 2L phosphorene has some states that cross E_f, suggesting metallization of the unexposed 2L phosphorene.

We show the partial density of states (PDOS) of the 3L phosphorene-metal systems and pure 3L phosphorene in Fig. 6. The band gap disappears for all eight systems, indicating the hybridization of the band structure and the metallization of 3L phosphorene. As expected, the change of PDOS in the strong chemical bonding case (the 3L phosphorene-Pd, Ni, Cr, and Ti systems) is more obvious than that in the weak chemical bonding case (the 3L phosphorene-Al, Ag, Au, and Cu systems).

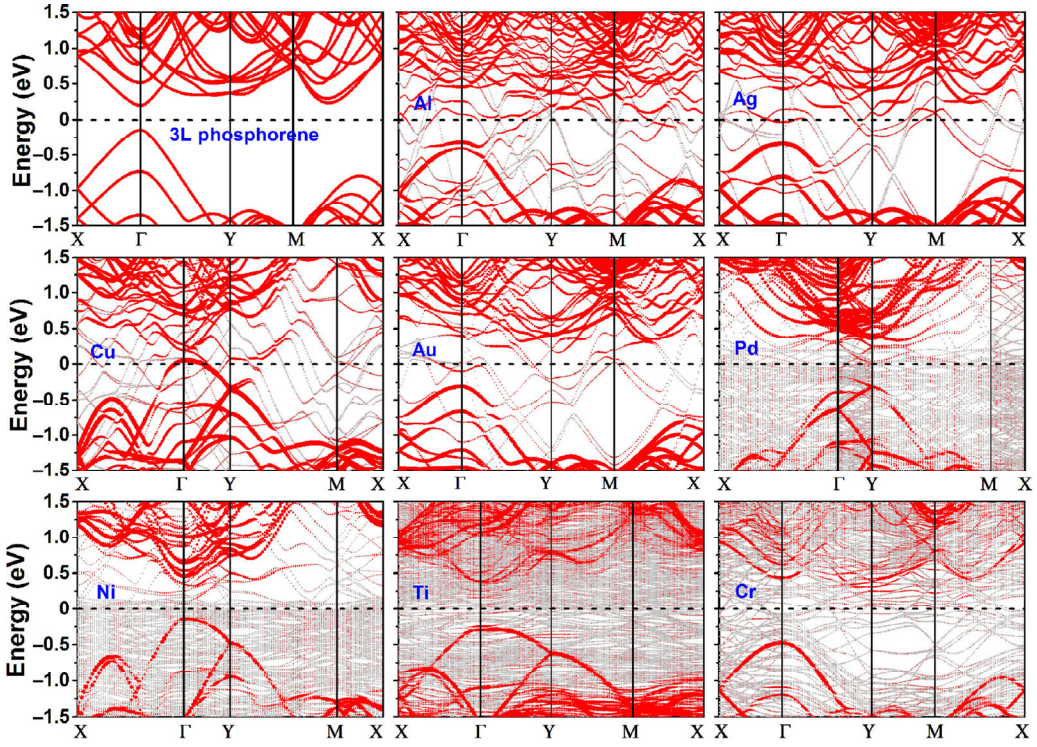

Figure 3 Band structures of pure 3L phosphorene and the 3L phosphorene-metal systems (projected to the 3L phosphorene). Gray line: Band structure of the interfacial systems; red line: Band structures projected to the 3L phosphorene. The line width is proportional to the weight. The band structures of pure 3L phosphorene are calculated in a $\sqrt{(2\boldsymbol{a})^2+\boldsymbol{b}^2} \times \sqrt{\boldsymbol{a}^2+\boldsymbol{b}^2}$ supercell. The Fermi level is set at zero energy and is denoted by black dashed line.

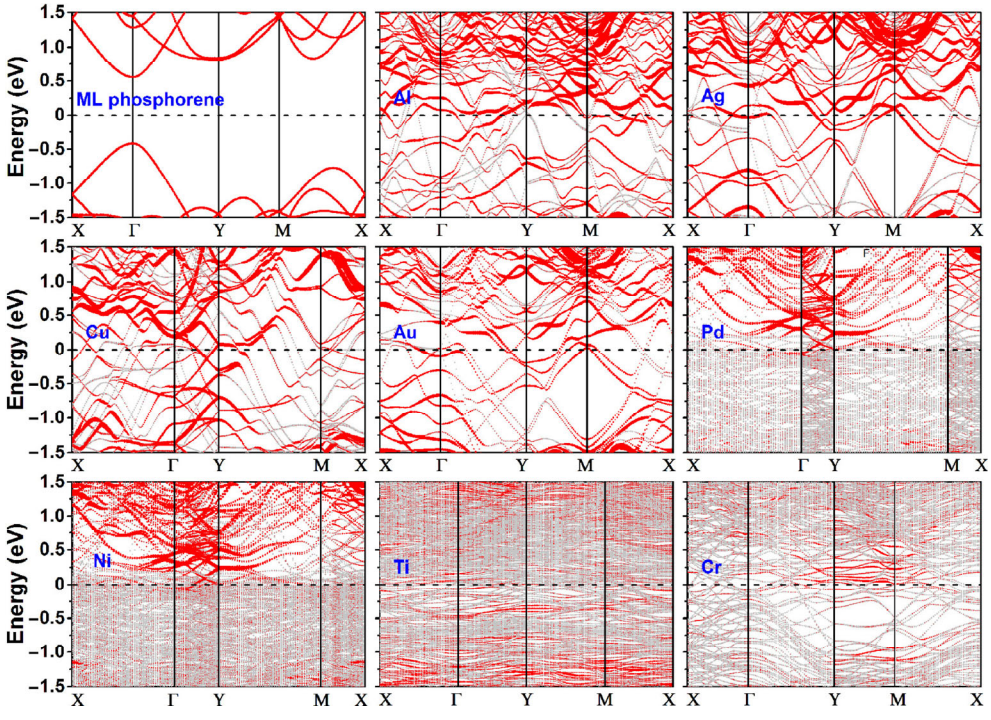

Figure 4 Band structures of pure ML phosphorene and the 3L phosphorene-metal systems (projected to the contacted phosphorene layer). Gray line: Band structure of the interfacial systems; red line: Band structures projected to the contacted phosphorene layer. The line width is proportional to the weight. The band structures of pure ML phosphorene are calculated in a $\sqrt{(2\boldsymbol{a})^2+\boldsymbol{b}^2} \times \sqrt{\boldsymbol{a}^2+\boldsymbol{b}^2}$ supercell. The Fermi level is set at zero energy and is denoted by black dashed lines.

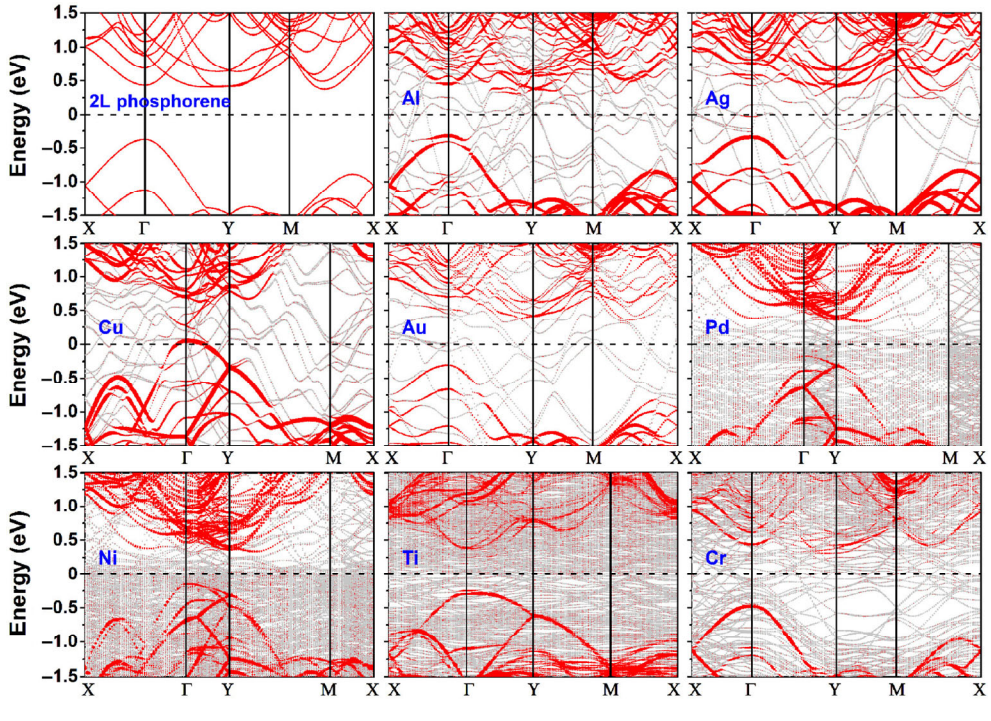

Figure 5 Band structures of pure 2L phosphorene and the 3L phosphorene-metal systems (projected to the unexposed 2L phosphorene). Gray line: Band structure of the interfacial systems; red line: Band structures projected to the unexposed 2L phosphorene. The line width is proportional to the weight. The band structures of pure 2L phosphorene are calculated in a $\sqrt{(2\boldsymbol{a})^2+\boldsymbol{b}^2} \times \sqrt{\boldsymbol{a}^2+\boldsymbol{b}^2}$ supercell. The Fermi level is set at zero energy and is denoted by black dashed lines.

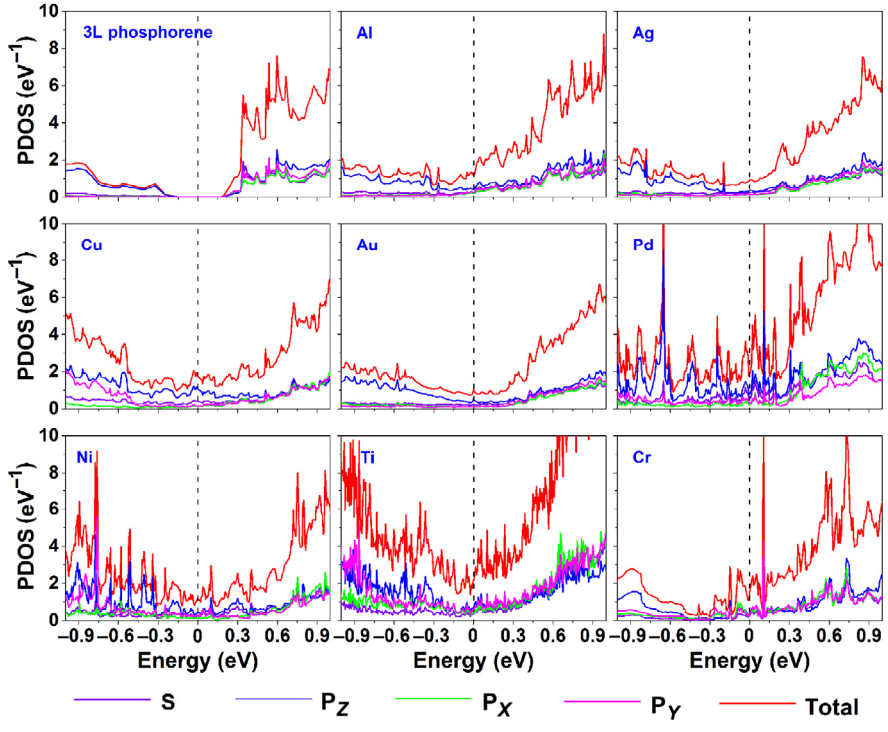

Figure 6 PDOS of pure 3L phosphorene and 3L phosphorene on the metal surfaces from the energy band calculations. The Fermi level is set at zero energy and is denoted by vertical black dashed lines.

The total electron distribution of 3L phosphorene-Ag, Cu, Ni, and Ti in real space is shown in Figs. 1(b)–1(e) respectively. More electrons accumulate at the interface of the 3L phosphorene-Ni and Ti systems than the 3L phosphorene-Ag and Cu systems, indicating the formation of a strong covalent bond between 3L phosphorene and Ni and Ti and a weak covalent bond between 3L phosphorene and Ag and Cu. d_{min} is slightly smaller than the sum of the single-bond covalent radii for phosphorous and metal atoms [53] ($r_P + r_M$) (Table 1) for the 3L phosphorene-Pd, Ni, Ti, and Cr systems, indicating the formation of strong covalent bond between phosphorene and Pd, Ni, Ti, and Cr. On the other hand, d_{min} is slightly larger than ($r_P + r_M$) for the 3L phosphorene-Al, Ag, Au, and Cu systems, indicating the formation of weak covalent bond between phosphorene and Al, Ag, Au, and Cu.

3.3 Vertical Schottky barrier height from the band structure

It is important to study the Schottky barrier and tunnel barrier of an FET. A schematic diagram of a 3L phosphorene FET is shown in Fig. 7. There are three different interfaces where a Schottky barrier can appear in a 3L phosphorene FET: The first is the contacted phosphorene layer and the metal (interface A in Fig. 7) in the vertical direction, with the corresponding SBH labeled as $\Phi^{3L}_{1,V}$; the second is between the contacted phosphorene layer and the unexposed 2L phosphorene (interface B in Fig. 7) in the vertical direction, with the corresponding SBH for hole (electron) labeled as $\Phi^{h,3L}_{23,V}$ ($\Phi^{e,3L}_{23,V}$); the third is between the electrode and the channel (interface C in Fig. 7) in the lateral direction, with the corresponding SBH for hole (electron) labeled as $\Phi^{h,3L}_{T,L}$ ($\Phi^{e,3L}_{T,L}$). Furthermore, a tunneling barrier can appear at interfaces A and B when electrons cross the interface between metal and 3L phosphorene.

The metallization of all the contacted phosphorene layers leads to the absence of a Schottky barrier at interface A ($\Phi^{3L}_{1,V} = 0$ eV) for all the studied phosphorene-metal systems. Electrons and holes still need to overcome a Schottky barrier if they cross interface B in all the studied phosphorene-metal systems, except in the 3L phosphorene-Cu system where the unexposed 2L phosphorene also undergoes a metallization. $\Phi^{e,3L}_{23,V}$ and $\Phi^{h,3L}_{23,V}$ are shown in Table 1.

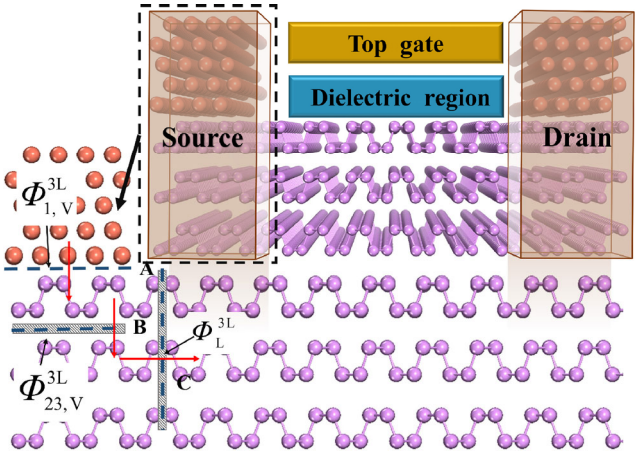

Figure 7 Right: Schematic diagram of a 3L phosphorene FET. Left: Schematic cross-sectional view of a typical metal contact to the intrinsic 3L phosphorene channel. A, B and C are the three interfaces (blue dashed lines) where Schottky barriers may exist. Red rows show the pathway that the electrons or holes transfer through the A, B, and C interfaces. Gray shadow represents interfacial states at the relevant interface. $\Phi^{3L}_{1,V}$, $\Phi^{3L}_{23,V}$, Φ^{3L}_{L} and represent the SBHs at the interface A, B, and C, respectively.

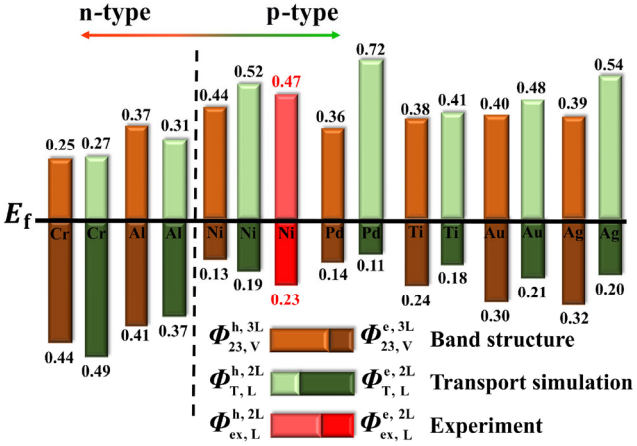

Figure 8 Comparison of the SBHs between the band structure results in the vertical direction for the 3L phosphorene FETs ($\Phi^{e/h,3L}_{23,V}$) and the quantum transport simulations ($\Phi^{e/h,2L}_{T,L}$) and the experimental observations ($\Phi^{e/h,2L}_{ex,L}$) in the lateral direction for the 2L phosphorene FETs.

We compare with those obtained from the 2L phosphorene quantum transport simulations in the lateral direction [28] and observation ($\Phi^{e,2L}_{T,L}$ for an electron and $\Phi^{h,2L}_{T,L}$ for a hole) [2] in Fig. 8. Both calculations show that 2L phosphorene forms n-type Schottky contacts with Cr and Al and p-type Schottky contacts with Ag, Au, Pd, Ni, and Ti, and that the theoretical polarity is the same as in experiments [1, 2, 17, 18, 23]. The SBHs from the two types of calculations are similar, and match with observations (0.23 eV for electron and 0.47 eV for hole) when Ni is used as electrode ($\Phi^{e,3L}_{23,V}$ = 0.13 eV and $\Phi^{h,3L}_{23,V}$ = 0.44 eV), as shown in Fig. 8 [2].

The similarity in the SBHs between the two types of calculations is not surprising. $\Phi^{e/h,3L}_{23,V}$ reflects the vertical SBH between the metalized first-layer phosphorene and the underlying semiconducting 2L phosphorene, while $\Phi^{h,2L}_{T,L}$ reflects the lateral SBH between the metalized first-layer phosphorene and the semiconducting channel 2L phosphorene. In both calculations, the coupling between the metalized first layer phosphorene and the semiconducting 2L phosphorene, which often lead to Fermi level pinning (FLP) [15, 16, 50–52, 54–56], has been fully taken into account by treating the metal and semiconducting parts as a whole in both models, despite their different interfacial states (Fig. 7). Hence, the lateral SBH in an *N*-layer 2D semiconducting material FET with a strongly interacting electrode can be estimated from a band structure analysis of its (*N* + 1)-layer counterpart. However, this method does not work for weakly interacting metal-semiconductor interfaces because the semiconductor below the metal electrodes is not metallized, and a Schottky barrier exists at the interface between the metal electrode and the (*N* + 1)-layer semiconductor underneath. The band gap of the (*N* + 1)-layer 2D semiconductor under the metal electrode is different from that of an *N*-layer 2D semiconductor. Therefore, in this case, the (*N* + 1)-layer vertical SBH cannot be used to estimate the lateral SBH of an *N*-layer 2D semiconductor FET.

The tunneling barriers can be inferred from the total potential profiles (Fig. 2) at the vertical 3L phosphorene-metal interfaces. There are no tunneling barriers at any of the interfaces of the 3L phosphorene-metal systems except in the 3L phosphorene-Cr system, where there is a small (0.50 eV) tunneling barrier at interface B (Fig. 7), as shown in Fig. 2(h) (the insert). These zero or small tunneling barriers are expected because 3L phosphorene is metallized when contacted with these metals.

3.4 Lateral SBH from quantum transport simulations and work function approximations

The metallized contacted phosphorene layer forms a

Schottky barrier with channel 3L phosphorene in the lateral direction, and the corresponding SBHs can be derived from the transmission spectrum of the 3L phosphorene FET. The transmission spectra of 3L phosphorene FETs in a two-probe model with eight different electrodes are depicted in Figs. 9(a)–9(d). Channel 3L phosphorene is found to be n-type doped with Ag and Cu electrodes, with electron SBHs of 0.16 and 0.28 eV, respectively. This finding is indicated by E_f being closer to the conduction-band minimum (CBM) of 3L phosphorene and the doping level increasing as the electron SBH decreases. In contrast, channel 3L phosphorene is p-type doped with Cr, Pd, Ni, Ti, Al, and Au electrodes, and has hole SBHs of 0.05, 0.11, 0.20, 0.30, 0.30, and 0.31 eV (Fig. 10(a)), respectively. These results occur because E_f is closer to the valence-band maximum (VBM) of 3L phosphorene, and the doping level increases as the hole SBH decreases. Consistently, the experiments observe n-type doping of FL phosphorene with Cu adatoms [29], and p-type doping of FL phosphorene with Au, Ti, Ni, and Pd electrodes [4, 6, 17].

The conclusion that the hole SBH of the Pd electrode (0.11 eV) is smaller than the Ni electrode (0.30 eV) is supported by the observation of a smaller contact resistance with a Pd electrode than with an Ni electrode [17]. More importantly, the observed electron (hole) SBH of 0.40 (0.21) eV in the 3L phosphorene FET with an Ni electrode [2] is in good agreement with our calculated result of 0.48 (0.20) eV. The observed hole SBH of 0.21 eV in FL phosphorene FET (thicker than 2 nm) with a Ti electrode [3] is also comparable with our calculated value of 0.30 eV. Furthermore, the observed p-type Ohmic contact in an FL phosphorene FET with Cr electrode is similar to our simulation result of a hole SBH of 0.05 eV for a Cr electrode [1]. These agreements support the accuracy of our quantum transport simulations. The SBHs of the 3L phosphorene FET are indeed generally smaller than the ML phosphorene FET due to the band gap of 3L phosphorene being smaller than that of ML phosphorene. The average electron/hole SBHs of the 3L phosphorene FETs are 0.13/0.31 eV smaller than those of their ML counterparts [14]. The transmission gap E_g is defined as the sum of the hole and electron SBHs; in other words, $E_g = \Phi_{T,L}^{h,3L} + \Phi_{T,L}^{e,3L}$. The transmission gaps for the 3L phosphorene FETs are 0.61, 0.63, 0.64, 0.66, 0.68, 0.68, 0.71, and 0.77 eV with Ag, Ti, Au, Pd, Cr, Ni, Cu,

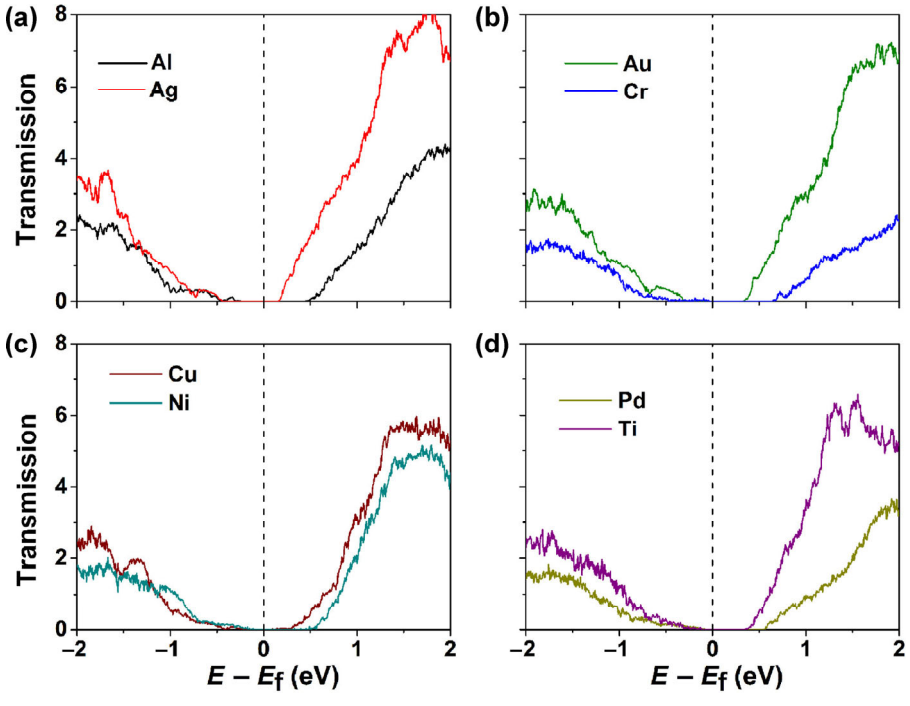

Figure 9 Zero-bias transmission spectra of the 3L phosphorene FETs with (a) Al, Ag, (b) Au, Cr, (c) Cu, Ni, (d) Pd and Ti electrodes and with a channel length of L = 5 nm.

and Al electrodes, respectively, compared with the experimental transmission gap of 0.61 eV with Ni electrodes [2].

The lateral SBH can also be obtained from the difference between the work functions of the 3L phosphorene-metal interfaces and the CBM and VBM of the pure 3L phosphorene. This method is called the work function approximation (WFA) method. The SBHs obtained from the WFA method, quantum transport simulations, and experiments are displayed in Fig. 10(a). The SBHs from the WFA show that 3L phosphorene forms p-type Schottky contacts with Ag and Ti with hole SBHs of 0.13 and 0.09 eV, respectively; n-type Schottky contacts with Al with electron SBH of 0.04 eV; and p-type Ohmic contact with Au, Cu, Ni, Cr, and Pd. However, both the quantum transport simulations and experiments demonstrate that Pd and Ni form p-type Schottky contacts instead of Ohmic contact with FL phosphorenes. The quantum transport simulation method gives more accurate SBH values than the WFA because the WFA method does not consider the interaction between the channel 3L phosphorene and the metal electrodes. This interaction results in FLP, which makes it difficult for 3L phosphorene to form an Ohmic contact with metal electrodes.

We plot the SBHs from the quantum transport simulation and the WFA as a function of the metal work functions in Figs. 10(b) and 10(c). The slopes of the straight lines fitted to the SBH-metal work function relations are far from 1, indicating a strong FLP. Moreover, the slope of the lines fitted to the functions

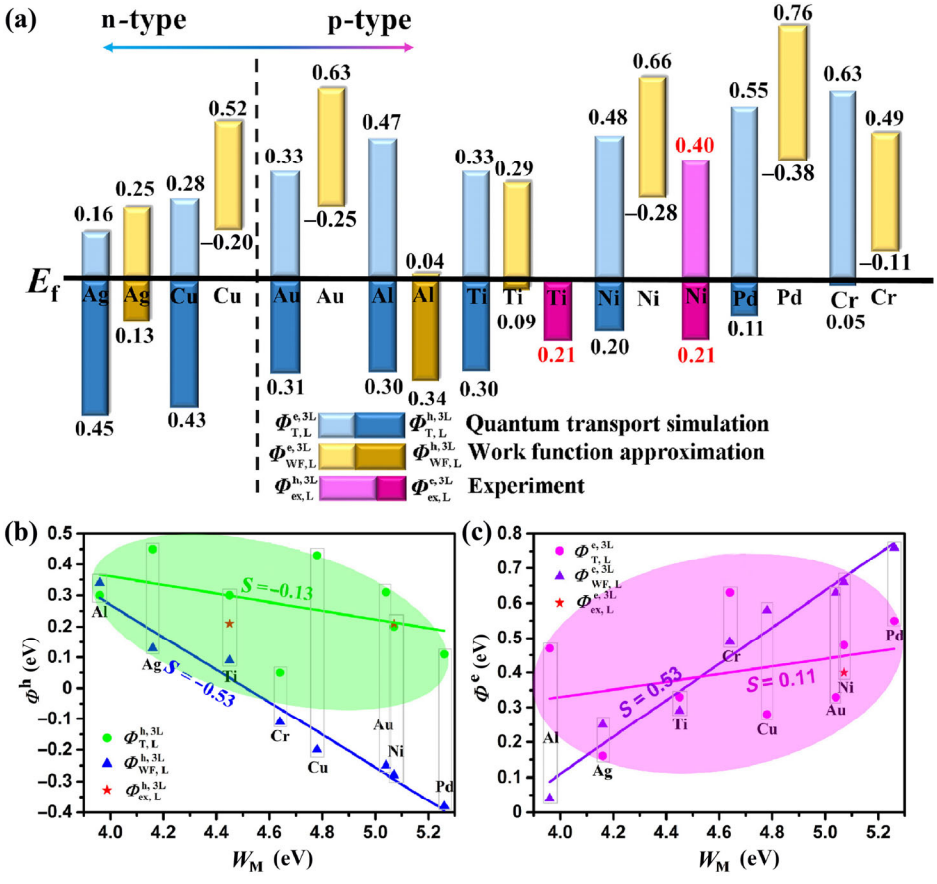

Figure 10 (a) 3L phosphorene SBHs in the lateral direction obtained from the quantum transport simulation and the WFA methods. The experimental SBHs with Ni and Ti (few layer thicker than 2 nm) as electrodes are also provided for comparison. (b) and (c) 3L phosphorene SBHs for hole (b) hole and electron (c) as a function of the metal work functions. The green and pink transparent ellipses are the smallest ellipses that can overcome all the SBHs of holes and electrons from the quantum transport simulations, respectively. The green and pink straight lines are the fitting lines for the SBHs of holes and electrons from the quantum transport simulations, respectively, and the blue and purple straight lines are the fitting lines for the SBHs of holes and electrons from the WFA, respectively.

of the SBHs from the WFA vs. the metal work functions (0.53 for electron SBH and −0.53 for hole SBHs) are much larger than those of the SBHs from the quantum transport simulations vs. the metal work functions (0.11 for electrons and −0.14 for holes SBHs) because WFA does not consider the interaction between the 3L phosphorene channel and the metal electrodes, and this interaction would result in further FLP.

Local device density of states (LDDOS) is a direct way to reflect the electron distribution in an FET, and the LDDOS of the 3L phosphorene FETs with Ag, Au, Cu, and Cr electrodes are shown in Fig. 11. There are metal-induced gap states (MIGS) in the channel for the 3L phosphorene FET with a Cr electrode, which are responsible for the strong FLP between the Cr electrode and phosphorene (namely, the SBHs calculated from the WFA, and direct quantum transport simulation differs greatly) [14]. 3L phosphorene forms n-type Schottky contacts with an electron SBH of 0.13 and 0.19 eV when Cu and Ag are used as electrodes, respectively, and the band bends downward due to an electron transfer from the electrode to the channel. 3L phosphorene forms p-type Schottky contacts with a hole SBH of 0.08 and 0.20 eV when Cr and Ni are used as electrodes, respectively, and the band bends upward due to an electron transfer from the channel to the electrode. The SBHs obtained from the LDDOS are comparable with the SBHs obtained from the transmission spectrum for the 3L phosphorene FET calculation.

Our FET uses top-contact electrodes, but for 3L phosphorene FETs, an edge contact can contact all layers of 3L phosphorene. The edge contact electrode only occupied a small space, which is critical for device minimization. However, if the number of atoms across the contact area is much larger than those along the contact edge, the top contact may be better than the edge contact because of its contact area. A combination of the two contacts may be a better choice [13]. Therefore, the edge contact and the combination of the top contact and edge contact is worthy of further study.

The strong FLP caused by the strong interaction between the 2D semiconductors and bulk metal electrodes is a serious problem for the development of 2D semiconductor Schottky barrier FETs (SBFETs). Recently, a vdW metal-semiconductor junction has been fabricated using 2D metals [57–59]. For example,

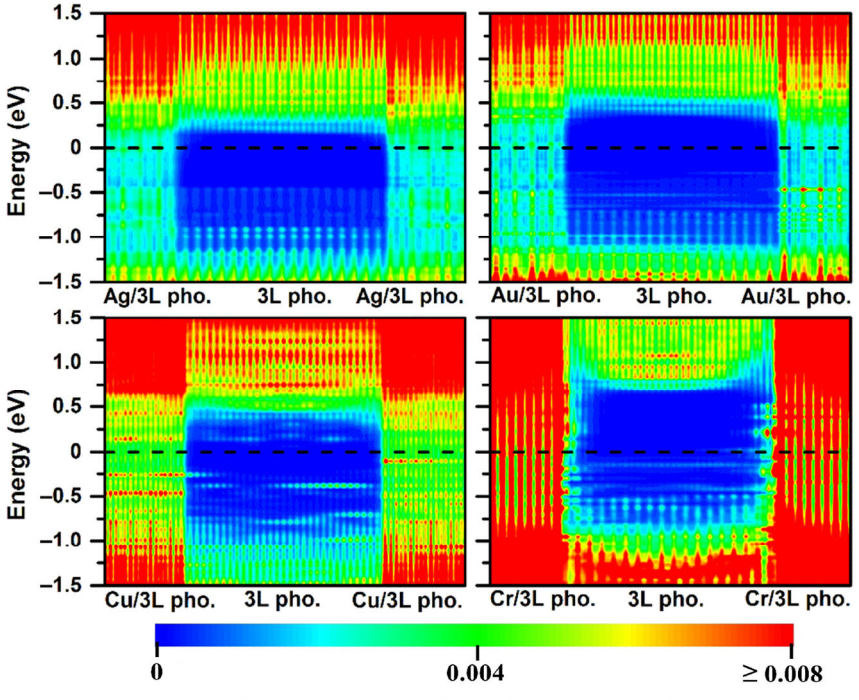

Figure 11 LDDOS in color coding for the 3L phosphorene FETs with Ag, Cu, Ni, and Cr electrodes and a channel length of L = 5 nm. The smaller SBH is indicated.

2D metallic T-MoS_2, T-WS_2, H-VS_2, and T-VS_2 contact with semiconducting H-MoS_2 [60], graphene contacts with phosphorene [61–63], O, OH, or F-doped 2D metal carbides and nitrides (MXenes) contact with WSe_2 [64]. These vdW metal-semiconductor junctions have been demonstrated to have fewer MIGS, which weakens the FLP, potentially reducing the SBH and suppressing e–h recombination at the interface. A graphene electrode has been used for phosphorene FETs, greatly improving the performance of the SBFET compared with bulk metal electrodes [61–63, 65]. Inserting a 2D material between phosphorene and the bulk metal electrode is an alternative approach to reducing the SBH, and related work is underway to reduce the SBH between phosphorene and the bulk metal electrode.

4 Conclusions

We have systematically calculated the interfacial properties of 3L phosphorene FETs with eight different metal electrodes. The contacted phosphorene layer is metallized, while unexposed 2L phosphorene is not metallized. There is a Schottky barrier at the interface between the contacted phosphorene layer and the unexposed 2L phosphorene in 3L phosphorene-metal systems, except for the phosphorene-Cu system. The SBHs in the vertical direction obtained from the band structures projected to the unexposed 2L phosphorene are consistent with those obtained from the quantum transport simulations and the experiments on 2L phosphorene FETs in the lateral direction. Therefore, the lateral SBH in an N-layer 2D semiconducting material FET with a strongly interacting electrode can be inferred from a band structure analysis of its $(N + 1)$-layer counterpart. The quantum transport simulations show that 3L phosphorene FETs with Ag and Cu electrodes have n-type Schottky contacts with electron SBHs of 0.16 and 0.28 eV in the lateral direction, respectively; while those with Cr, Pd, Ni, Ti, Al, and Au electrodes have p-type Schottky contacts with hole SBHs of 0.05, 0.11, 0.20, 0.30, 0.30, and 0.31 eV in the lateral direction, respectively. The theoretical polarity and SBHs of the 3L phosphorene FETs generally agree with the existing experiment.

Acknowledgements

This work was supported by the National Natural Science Foundation of China (NSFC) (Nos. 11274016, 11474012, 11674005 and 11274233), the National Basic Research Program of China (973 Program) (Nos. 2013CB932604 and 2012CB619304), the Ministry of Science and Technology of China (Nos. 2016YFB0700600 and 2016YFA0301300), and open Fund of Key Laboratory for Intelligent Nano Materials and Devices of the Ministry of Education of China (No. INMD-2016M03).

References

[1] Li, L. K.; Yu, Y. J.; Ye, G. J.; Ge, Q. Q.; Ou, X. D.; Wu, H.; Feng, D. L.; Chen, X. H.; Zhang, Y. B. Black phosphorus field-effect transistors. *Nat. Nanotechnol.* **2014**, *9*, 372–377.

[2] Das, S.; Zhang, W.; Demarteau, M.; Hoffmann, A.; Dubey, M.; Roelofs, A. Tunable transport gap in phosphorene. *Nano Lett.* **2014**, *14*, 5733–5739.

[3] Liu, H.; Neal, A. T.; Zhu, Z.; Luo, Z.; Xu, X. F.; Tománek, D.; Ye, P. D. Phosphorene: An unexplored 2D semiconductor with a high hole mobility. *ACS Nano* **2014**, *8*, 4033–4041.

[4] Das, S.; Demarteau, M.; Roelofs, A. Ambipolar phosphorene field effect transistor. *ACS Nano* **2014**, *8*, 11730–11738.

[5] Reich, E. S. Phosphorene excites materials scientists. *Nature* **2014**, *506*, 19.

[6] Buscema, M.; Groenendijk, D. J.; Blanter, S. I.; Steele, G. A.; van der Zant, H. S. J.; Castellanos-Gomez, A. Fast and broadband photoresponse of few-layer black phosphorus field-effect transistors. *Nano Lett.* **2014**, *14*, 3347–3352.

[7] Zhang, S.; Yang, J.; Xu, R. J.; Wang, F.; Li, W. F.; Ghufran, M.; Zhang, Y. W.; Yu, Z. F.; Zhang, G.; Qin, Q. H. et al. Extraordinary photoluminescence and strong temperature/angle-dependent Raman responses in few-layer phosphorene. *ACS Nano* **2014**, *8*, 9590–9596.

[8] Churchill, H. O.; Jarillo-Herrero, P. Two-dimensional crystals: Phosphorus joins the family. *Nat. Nanotechnol.* **2014**, *9*, 330–331.

[9] Koenig, S. P.; Doganov, R. A.; Schmidt, H.; Castro Neto, A. H.; Özyilmaz, B. Electric field effect in ultrathin black phosphorus. *Appl. Phys. Lett.* **2014**, *104*, 103106.

[10] Wan, R. L.; Cao, X.; Guo, J. Simulation of phosphorene Schottky-barrier transistors. *Appl. Phys. Lett.* **2014**, *105*, 163511.

[11] Allain, A.; Kang, J. H.; Banerjee, K.; Kis, A. Electrical contacts to two-dimensional semiconductors. *Nat. Mater.* **2015**, *14*, 1195–1205.

[12] Liu, H.; Du, Y. C.; Deng, Y. X.; Ye, P. D. Semiconducting black phosphorus: Synthesis, transport properties and electronic applications. *Chem. Soc. Rev.* **2015**, *44*, 2732–2743.

[13] Kang, J. H.; Liu, W.; Sarkar, D.; Jena, D.; Banerjee, K. Computational study of metal contacts to monolayer transition-metal dichalcogenide semiconductors. *Phys. Rev. X* **2014**, *4*, 031005.

[14] Pan, Y. Y.; Wang, Y. Y.; Ye, M.; Quhe, R. G.; Zhong, H. X.; Song, Z. G.; Peng, X. Y.; Yu, D. P.; Yang, J. B.; Shi, J. J. et al. Monolayer phosphorene–metal contacts. *Chem. Mater.* **2016**, *28*, 2100–2109.

[15] Zhong, H. X.; Quhe, R. G.; Wang, Y. Y.; Ni, Z. Y.; Ye, M.; Song, Z. G.; Pan, Y. Y.; Yang, J. B.; Yang, L.; Lei, M. et al. Interfacial properties of monolayer and bilayer MoS_2 contacts with metals: Beyond the energy band calculations. *Sci. Rep.* **2016**, *6*, 21786.

[16] Wang, Y. Y.; Yang, R. X.; Quhe, R. G.; Zhong, H. X.; Cong, L. X.; Ye, M.; Ni, Z. Y.; Song, Z. G.; Yang, J. B.; Shi, J. J. et al. Does p-type ohmic contact exist in WSe_2-metal interfaces? *Nanoscale* **2016**, *8*, 1179–1191.

[17] Du, Y. C.; Liu, H.; Deng, Y. X.; Ye, P. D. Device perspective for black phosphorus field-effect transistors: Contact resistance, ambipolar behavior, and scaling. *ACS Nano* **2014**, *8*, 10035–10042.

[18] Perello, D. J.; Chae, S. H.; Song, S.; Lee, Y. H. High-performance n-type black phosphorus transistors with type control via thickness and contact-metal engineering. *Nat. Commun.* **2015**, *6*, 7809.

[19] Wang, H.; Wang, X. M.; Xia, F. N.; Wang, L. H.; Jiang, H.; Xia, Q. F.; Chin, M. L.; Dubey, M.; Han, S. J. Black phosphorus radio-frequency transistors. *Nano Lett.* **2014**, *14*, 6424–6429.

[20] Wan, B. S.; Yang, B. C.; Wang, Y.; Zhang, J. Y.; Zeng, Z. M.; Liu, Z. Y.; Wang, W. H. Enhanced stability of black phosphorus field-effect transistors with SiO_2 passivation. *Nanotechnol.* **2015**, *26*, 435702.

[21] Li, X. F.; Du, Y. C.; Si, M. W.; Yang, L. M.; Li, S. C.; Li, T. Y.; Xiong, X.; Ye, P. D.; Wu, Y. Q. Mechanisms of current fluctuation in ambipolar black phosphorus field-effect transistors. *Nanoscale* **2016**, *8*, 3572–3578.

[22] Buscema, M.; Groenendijk, D. J.; Steele, G. A.; van der Zant, H. S.; Castellanos-Gomez, A. Photovoltaic effect in few-layer black phosphorus PN junctions defined by local electrostatic gating. *Nat. Commun.* **2014**, *5*, 4651.

[23] Xia, F. N.; Wang, H.; Jia, Y. C. Rediscovering black phosphorus as an anisotropic layered material for optoelectronics and electronics. *Nat. Commun.* **2014**, *5*, 4458.

[24] Liu, H.; Neal, A. T.; Si, M. W.; Du, Y. C.; Ye, P. D. The effect of dielectric capping on few-layer phosphorene transistors: Tuning the Schottky barrier heights. *IEEE Electr. Device Lett.* **2014**, *35*, 795–797.

[25] Xu, R. J.; Yang, J.; Zhu, Y.; Yan, H.; Pei, J. J.; Myint, Y. W.; Zhang, S.; Lu, Y. R. Layer-dependent surface potential of phosphorene and anisotropic/layer-dependent charge transfer in phosphorene-gold hybrid systems. *Nanoscale* **2015**, *8*, 129–135.

[26] Gong, K.; Zhang, L.; Ji, W.; Guo, H. Electrical contacts to monolayer black phosphorus: A first-principles investigation. *Phys. Rev. B* **2014**, *90*, 125441.

[27] Zhu, S. C.; Ni, Y.; Liu, J.; Yao, K. L. The study of interaction and charge transfer at black phosphorus–metal interfaces. *J. Phys. D Appl. Phys.* **2015**, *48*, 445101.

[28] Pan, Y. Y.; Dan, Y.; Wang, Y. Y.; Ye, M.; Zhang, H.; Quhe, R. G.; Zhang, X. Y.; Li, J. Z.; Guo, W. L.; Yang, L. et al. Schottky barriers in bilayer phosphorene transistors. *ACS Appl. Mater. Interfaces* **2017**, *9*, 12694–12705.

[29] Koenig, S. P.; Doganov, R. A.; Seixas, L.; Carvalho, A.; Tan, J. Y.; Watanabe, K.; Taniguchi, T.; Yakovlev, N.; Neto, A. H. C.; Ozyilmaz, B. Electron doping of ultrathin black phosphorus with Cu adatoms. *Nano Lett.* **2016**, *16*, 2145–2151.

[30] Yuan, Y. K.; Quhe, R. G.; Zheng, J. X.; Wang, Y. Y.; Ni, Z. Y.; Shi, J. J.; Lu, J. Strong band hybridization between silicene and Ag(111) substrate. *Physica E* **2014**, *58*, 38–42.

[31] Cheng, D. J.; Barcaro, G.; Charlier, J. C.; Hou, M.; Fortunelli, A. Homogeneous nucleation of graphitic nanostructures from carbon chains on Ni(111). *J. Phy. Chem. C* **2011**, *115*, 10537–10543.

[32] So, C.; Zhang, H.; Wang, Y.; Ye, M.; Pan, Y.; Quhe, R.; Li, J. Z.; Zhang, X.; Zhou, Y.; Lu, J. A computational study of monolayer hexagonal WTe_2 to metal interfaces. *Phys. Status Solidi B* **2017**, in press, DOI: 10.1002/pssb.201600837.

[33] Qiao, J. S.; Kong, X. H.; Hu, Z. X.; Yang, F.; Ji, W. High-mobility transport anisotropy and linear dichroism in few-layer black phosphorus. *Nat. Commun.* **2014**, *5*, 4475.

[34] Kresse, G.; Joubert, D. From ultrasoft pseudopotentials to the projector augmented-wave method. *Phys. Rev. B* **1999**, *59*, 1758–1775.

[35] Monkhorst, H. J.; Pack, J. D. Special points for Brillouin-zone integrations. *Phys. Rev. B* **1976**, *13*, 5188–5192.

[36] Kresse, G.; Hafner, J. *Ab initio* molecular dynamics for liquid metals. *Phys. Rev. B* **1993**, *47*, 558–561.

[37] Kresse, G.; Furthmüller, J. Efficient iterative schemes for *ab initio* total-energy calculations using a plane-wave basis set. *Phys. Rev. B* **1996**, *54*, 11169–11186.

[38] Klimeš, J.; Bowler, D. R.; Michaelides, A. Chemical accuracy for the van der Waals density functional. *J. Phys.* **2010**, *22*, 022201.

[39] Segall, M. D.; Lindan, P. J. D.; Probert, M. J.; Pickard, C. J.; Hasnip, P. J.; Clark, S. J.; Payne, M. C. First-principles simulation: Ideas, illustrations and the CASTEP code. *J. Phys.* **2002**, *14*, 2717–2744.

[40] Taylor, J.; Guo, H.; Wang, J. *Ab initio* modeling of quantum transport properties of molecular electronic devices. *Phys. Rev. B* **2001**, *63*, 245407.

[41] Brandbyge, M.; Mozos, J. L.; Ordejón, P.; Taylor, J.; Stokbro, K. Density-functional method for nonequilibrium electron transport. *Phys. Rev. B* **2002**, *65*, 165401.

[42] Çakır, D.; Peeters, F. M. Dependence of the electronic and transport properties of metal-$MoSe_2$ interfaces on contact structures. *Phys. Rev. B* **2014**, *89*, 245403.

[43] Perdew, J. P.; Burke, K.; Ernzerhof, M. Generalized gradient approximation made simple. *Phys. Rev. Lett.* **1996**, *77*, 3865–3868.

[44] Wang, Y. Y.; Huang, P.; Ye, M.; Quhe, R. G.; Pan, Y. Y.; Zhang, H.; Zhong, H. X.; Shi, J. J.; Lu, J. Many-body effect, carrier mobility, and device performance of hexagonal arsenene and antimonene. *Chem. Mater.* **2017**, *29*, 2191–2201.

[45] Guo, Y.; Pan, F.; Ye, M.; Wang, Y. Y.; Pan, Y. Y.; Zhang, X. Y.; Li, J. Z.; Zhang, H.; Lu, J. Interfacial properties of stanene–metal contacts. *2D Mater.* **2016**, *3*, 035020.

[46] Zhong, H. X.; Quhe, R. G.; Wang, Y. Y.; Shi, J. J.; Lü, J. Silicene on substrates: A theoretical perspective. *Chin. Phys. B* **2015**, *24*, 087308.

[47] Zhao, J. J.; Liu, H. S.; Yu, Z. M.; Quhe, R. G.; Zhou, S.; Wang, Y. Y.; Liu, C. C.; Zhong, H. X.; Han, N. N.; Lu, J. et al. Rise of silicene: A competitive 2D material. *Prog. Mater. Sci.* **2016**, *83*, 24–151.

[48] Quhe, R. G.; Yuan, Y. K.; Zheng, J. X.; Wang, Y. Y.; Ni, Z. Y.; Shi, J. J.; Yu, D. P.; Yang, J. B.; Lu, J. Does the Dirac cone exist in silicene on metal substrates? *Sci. Rep.* **2014**, *4*, 5476.

[49] Kang, J. H.; Liu, W.; Banerjee, K. High-performance MoS_2 transistors with low-resistance molybdenum contacts. *Appl. Phys. Lett.* **2014**, *104*, 093106.

[50] Ni, Z. Y.; Ye, M.; Ma, J. H.; Wang, Y. Y.; Quhe, R. G.; Zheng, J. X.; Dai, L.; Yu, D. P.; Shi, J. J.; Yang, J. B. et al. Performance upper limit of sub-10 nm monolayer MoS_2 transistors. *Adv. Electron. Mater.* **2016**, *2*, 1600191.

[51] Pan, Y. Y.; Wang, Y. Y.; Wang, L.; Zhong, H. X.; Quhe, R. G.; Ni, Z. Y.; Ye, M.; Mei, W. N.; Shi, J. J.; Guo, W. L. et al. Graphdiyne-metal contacts and graphdiyne transistors. *Nanoscale* **2015**, *7*, 2116–2127.

[52] Pan, Y. Y.; Li, S. B.; Ye, M.; Quhe, R. G.; Song, Z. G.; Wang, Y. Y.; Zheng, J. X.; Pan, F.; Guo, W. L.; Yang, J. B. et al. Interfacial properties of monolayer $MoSe_2$–metal contacts. *J. Phys. Chem. C* **2016**, *120*, 13063–13070.

[53] Pyykkö, P.; Atsumi, M. Molecular single-bond covalent radii for elements 1–118. *Chem. Eur. J.* **2008**, *15*, 186–197.

[54] Van Hoof, C.; Deneffe, K.; De Boeck, J.; Arent, D. J.; Borghs, G. Franz–Keldysh oscillations originating from a well-controlled electric field in the GaAs depletion region. *Appl. Phys. Lett.* **1989**, *54*, 608–610.

[55] Shen, H.; Dutta, M.; Fotiadis, L.; Newman, P. G.; Moerkirk, R. P.; Chang, W. H.; Sacks, R. N. Photoreflectance study of surface Fermi level in GaAs and GaAlAs. *Appl. Phys. Lett.* **1990**, *57*, 2118–2120.

[56] Hwang, J. S.; Chang, C. C.; Chen, M. F.; Chen, C. C.; Lin, K. I.; Tang, F. C.; Hong, M.; Kwo, J. Schottky barrier height and interfacial state density on oxide-GaAs interface. *J. Appl. Phys.* **2003**, *94*, 348–353.

[57] Cho, S.; Kim, S.; Kim, J. H.; Zhao, J.; Seok, J.; Keum, D. H.; Baik, J.; Choe, D. H.; Chang, K. J.; Suenaga, K. et al. Phase patterning for ohmic homojunction contact in $MoTe_2$. *Science* **2015**, *349*, 625–628.

[58] Kim, A. R.; Kim, Y.; Nam, J.; Chung, H. S.; Kim, D. J.; Kwon, J. D.; Park, S. W.; Park, J.; Choi, S. Y.; Lee, B. H. et al. Alloyed 2D metal-semiconductor atomic layer junctions. *Nano Lett.* **2016**, *16*, 1890–1895.

[59] Kappera, R.; Voiry, D.; Yalcin, S. E.; Branch, B.; Gupta, G.; Mohite, A. D.; Chhowalla, M. Phase-engineered low-resistance contacts for ultrathin MoS_2 transistors. *Nat. Mater.* **2014**, *13*, 1128–1134.

[60] Liu, Y. Y.; Stradins, P.; Wei, S. H. Van der Waals metal-semiconductor junction: Weak Fermi level pinning enables effective tuning of Schottky barrier. *Sci. Adv.* **2016**, *2*, e1600069.

[61] Padilha, J. E.; Fazzio, A.; da Silva, A. J. R. Van der Waals heterostructure of phosphorene and graphene: Tuning the Schottky barrier and doping by electrostatic gating. *Phys. Rev. Lett.* **2015**, *114*, 066803.

[62] Avsar, A.; Vera-Marun, I. J.; Tan, J. Y.; Watanabe, K.; Taniguchi, T.; Neto, A. H. C.; Özyilmaz, B. Air-stable transport in graphene-contacted, fully encapsulated ultrathin black phosphorus-based field-effect transistors. *ACS Nano* **2015**, *9*, 4138–4145.

[63] Hu, W.; Wang, T.; Yang, J. L. Tunable Schottky contacts in hybrid graphene–phosphorene nanocomposites. *J. Mater. Chem. C* **2015**, *3*, 4756–4761.

[64] Liu, Y. Y.; Xiao, H.; Goddard III, W. A. Schottky-barrier-free contacts with two-dimensional semiconductors by surface-engineered MXenes. *J. Am. Chem. Soc.* **2016**, *138*, 15853–15856.

[65] Quhe, R. G.; Peng, X. Y.; Pan, Y. Y.; Ye, M.; Wang, Y. Y.; Zhang, H.; Feng, S. Y.; Zhang, Q. X.; Shi, J. J.; Yang, J. B. et al. Can a black phosphorus Schottky barrier transistor be good enough? *ACS Appl. Mater. Interfaces* **2017**, *9*, 3959–3966.